Intraplane to interplane optical interconnects with a high diffraction efficiency electro-optic grating

Degui Sun, Chunhe Zhao, and Ray T. Chen

We report on a new optical interconnect architecture for three-dimensional, multiple electro-optic gratings with $LiNbO_3$ used in conjunction with substrate guided waves. First the operating mechanism of the system is studied in detail, and the momentum mismatch in the operating process of the system is also demonstrated. We then derive a new method for calculating coupling efficiency by introducing a compensation for the mismatch. This theoretical research allows the new optical interconnect architecture to provide a higher design accuracy and an optimized coupling efficiency, even though it is under the case of momentum mismatch. We achieve this result by introducing a substrate guided wave with 45° bouncing angle and 100-V applied voltage. The successful design and its theoretical analysis will be helpful for research on the grating coupler. © 1997 Optical Society of America

Key words: Optical interconnection, electro-optic grating, momentum mismatch, phase compensation, coupling efficiency.

1. Introduction

The development of modern optical information processing technologies such as optical interconnection, memory, and computing requires multiplexed parallelism, high density, high switching speed and efficiency, and better controllability.[1–3] One of the most pivotal elements for the realization of these applications is electro-optic (EO) modulated phase grating that has been used to perform switching, numerical operations, and interconnections for computing and information processing.[4–6]

The EO modulated phase grating has received attention because of its important applications in optical interconnection, communication, memory, and computing.[7–11] However, the study of EO grating with high diffraction efficiency and short interaction length has not been investigated carefully because the momentum matching for high diffraction efficiency based on the Bragg diffraction theory is not easy to realize.[12] In this paper, we investigate a microstructural EO grating based on the $LiNbO_3$ crystal for a novel intraplane-to-interplane interconnect application. Substrate guided waves are employed to provide the signal, which may be data, image, etc., to be routed. In this research, not only do we study the operating mechanism of the system in detail and verify the momentum mismatch in the operation, but we also propose a new method for calculating coupling efficiencies by introducing a compensation for the mismatch. At the same time, an optimized architecture is obtained. Therefore the result presented provides not only a higher design accuracy, but also a high coupling efficiency. In Section 2, the bouncing angle θ_1 is selected in accordance with the total interreflection condition that the microstructural EO device requires without activating the EO grating. The diffraction angle that can break the total interreflection condition and the periodicity of the EO grating are discussed. Furthermore, we study the momentum mismatch of the system and discuss its influence on the coupling efficiency based on the Bragg diffraction theory (Section 3). To obtain the accurate design, the electric-field distribution and index modulation are briefly studied in Section 4. On that basis, in Section 5 a compensation method for the mismatch is proposed and analyzed, and the coupling efficiency is optimized by integration for index modulation. In Section 6, we provide our conclusions.

2. Determination of the Bouncing Angle in $LiNbO_3$

The purpose of this research is to study and design an EO grating with a short interaction length as shown

The authors are with the Department of Electrical and Computer Engineering, University of Texas at Austin, Austin, Texas 78712-1084.

Received 2 October 1995; revised manuscript received 22 July 1996.

0003-6935/97/030629-06$10.00/0

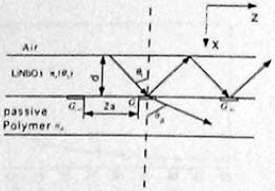

Fig. 1. Construction of $LiNbO_3$-based EO diffraction grating.

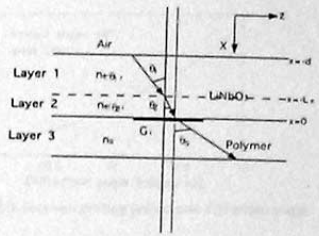

Fig. 2. Relationships among the unmodulated $LiNbO_3$ sublayer 1, the modulated layer 2, and the photopolymer memory layer 3.

in Fig. 1. $LiNbO_3$ is used to produce index modulation by the use of microelectrodes at various spots marked with G_i, whereas polymer is used to fulfill such required functions as wavelength redistribution and data storage and reading. When the EO grating is activated, the optical beams are coupled with high efficiency into the polymeric material when an appropriate voltage is applied. Otherwise the beams are total-internally reflected at these spots. This operating process is shown schematically in Fig. 2 in which the coupling process is performed between the first layer and the second layer. The second layer functions as an index modulation layer of grating, and its thickness L_e is the effective modulation depth of $LiNbO_3$ crystal. Of course the second layer does not exist when the EO grating is not activated and the bouncing is within the first layer. Therefore the first requirement is achieved by a bouncing angle θ_1 in $LiNbO_3$ that is bigger than its critical angle θ_c, and the second requirement is achieved by a diffraction angle θ_2 in the second layer of $LiNbO_3$ that is smaller than the critical angle θ_c. Therefore the bouncing beam within the $LiNbO_3$ substrate can be controlled by the given activated EO grating. In this research, we used ITO material as electrodes to obtain higher diffraction efficiency. Along the cutting direction of $LiNbO_3$ as shown in Figs. 1 and 2, the refractive index of $LiNbO_3$ is a function of the angle θ between the optical beam and the x axis and is defined as follows[12]:

$$\frac{1}{n_e^2(\theta)} = \frac{\sin^2\theta}{n_o^2} + \frac{\cos^2\theta}{n_e^2}, \tag{1}$$

and the critical angle for the total internal reflection can be calculated by

$$\theta_c = \arcsin\left[\frac{n_2}{n_e(\theta_1)}\right], \tag{2}$$

where $n_2 = 1.543$ is the refractive index of the photopolymer material. If we set $\theta_1 = 45°$, we can obtain $n_e(45°) = 2.24$ according to Eq. (1) and also $\theta_c = 43.49°$ according to Eq. (2). Apparently θ_1 is bigger than θ_c which meets the first requirement for the operations of the system.

3. The Electric-Field Distribution and its Influence on Index Modulation

As illustrated in Fig. 1, the electrode grating vector is along the z direction and the light wave travels within the z–x plane. When voltage V is applied across the electrodes and if the width of the spacing between the electrodes is $2a$, we have

$$\frac{\partial^2 V}{\partial z^2} + \frac{\partial^2 V}{\partial x^2} = 0, \tag{3a}$$

$$\varepsilon_z \frac{\partial^2 V}{\partial z^2} - \varepsilon_x \frac{\partial^2 V}{\partial x^2} = 0, \tag{3b}$$

where ε_z and ε_x are dielectric constants in directions z and x, respectively. By our using the coordinate transformation,

$$x' = \sqrt{\varepsilon_z/\varepsilon_x}\,x, \tag{4}$$

Eq. (3b) can also be written as

$$\frac{\partial^2 V}{\partial z^2} - \frac{\partial^2 V}{\partial x'^2} = 0. \tag{5}$$

By our using the following coordinate transformation again,

$$z = a \cosh u \cos v, \tag{6a}$$

$$x' = a \sinh u \sin v, \tag{6b}$$

the solutions for Eq. (5) can be written as[13]

$$E_z = -\left(\frac{U}{a\pi}\right)\frac{\cosh u \sin v}{\cosh^2 u - \cos^2 v}, \tag{7a}$$

$$E_x = -\left(\frac{U}{a\pi}\right)\frac{\sinh u \cos v}{\cosh^2 - \cos^2 v}\sqrt{\varepsilon_z/\varepsilon_x}. \tag{7b}$$

Eqs. (6) and (7) determine the distribution of electric-field components in directions z and x. Furthermore, together with Eq. (1), we can solve for the index modulation of $LiNbO_3$ induced by the electric field as follows:

$$\Delta n_e(\theta_1) = \frac{n_e^3 \sin^2\theta_1 \Delta n_o - n_o^3 \cos^2\theta_1 \Delta n_e}{(n_e^2 \cos^2\theta_1 + n_o^2 \sin^2\theta_1)^{3/2}}. \tag{8}$$

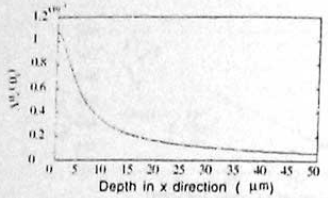

Fig. 3. Distribution curve of index modulation as a function of x.

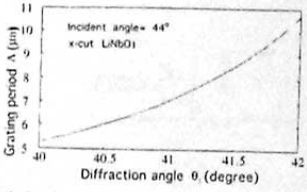

Fig. 5. Relationship between grating period and diffraction angle.

where Δn_e and Δn_o are calculated by

$$\Delta n_e = -\frac{1}{2} n_e^3 \gamma_{33} E_z, \tag{9a}$$

$$\Delta n_o = -\frac{1}{2} n_o^3 \gamma_{13} E_z, \tag{9b}$$

where γ_{33} and γ_{13} are the EO coefficients of the $LiNbO_3$ gratings. Because we study the coupling case in x direction, we discuss only the index modulation in x direction by taking $z = 0$. By combining Eqs. (8) and (9) we obtain the index modulation curve $\Delta n_e(x)$ with respect to x, as shown in Fig. 3. Note that the index modulation $\Delta n_e(\theta_1, x)$ dramatically decreases along x (depth) direction. Therefore it is necessary to use the integration to optimize the coupling efficiency.

4. Coupling Conditions and Momentum Mismatch of the Coupling System

In this system, the coupling of optical beams under the action of the EO grating is a key operation. Because some factors supporting the operation, such as the grating direction and period, the directions and amplitudes of wave vectors, and the index modulation of the $LiNbO_3$ crystal, are all limited by the system itself, coupling conditions and efficiency are worthy of a detailed study. As shown in Fig. 4, $\mathbf{K}_1$, $\mathbf{K}_2$, and $\mathbf{K}_g$ indicate the incident wave vector, the diffracted wave vector, and the grating vector, respectively. In z direction, we define

$$\beta_1 = \frac{2\pi}{\lambda} n_e(\theta_1)\sin\theta_1, \tag{10a}$$

$$\beta_2 = \frac{2\pi}{\lambda} n_e(\theta_2)\sin\theta_2, \tag{10b}$$

$$k_g = \frac{2\pi}{\Lambda}. \tag{10c}$$

In x direction, we define

$$\alpha_1 = \frac{2\pi}{\lambda} n_e(\theta_1)\cos\theta_1, \tag{11a}$$

$$\alpha_2 = \frac{2\pi}{\lambda} n_e(\theta_2)\cos\theta_2, \tag{11b}$$

where λ and Λ are the wavelength and the grating period, respectively. Based on the above equations, the momentum mismatches in both z and x directions are defined as follows:

$$\Delta\beta = \beta_1 - \beta_2 - mk_g, \tag{12}$$

$$\Delta\alpha = \alpha_2 - \alpha_1. \tag{13}$$

In the Bragg diffraction theory, the vectors that are only in the direction of the grating vector are required to be matched, i.e., $\Delta\beta = 0$.[12] According to Eqs. (10a), (10b) and (12), when $\Delta\beta = 0$, we can obtain the relationship between the grating period and the diffraction angle for the Bragg condition:

$$\Lambda = \frac{\lambda}{n_e(\theta_1)\sin\theta_1 - n_e(\theta_2)\sin\theta_2}. \tag{14}$$

Based on Eqs. (1) and (14), we obtain the relationship between grating period Λ and diffraction angle θ_2 as shown in Fig. 5 in which θ_2 is always smaller than the critical angle of 43.49° and that agrees with the second requirement of the system operation. It is certain that the value of $[n_e(\theta_2)\cos\theta_2 - n_e(\theta_1)\cos\theta_1]$ functions as the grating period Λ or diffraction angle θ_2. Note that all the allowable values of the grating period in Fig. 5 are able to be implemented practically. In terms of Bragg diffraction theory, if both $\Delta\beta$ and $\Delta\alpha$ are zero, three vectors, $\mathbf{K}_1$, $\mathbf{K}_2$, and $\mathbf{K}_g$ are matched, which is the perfect Bragg diffraction, and

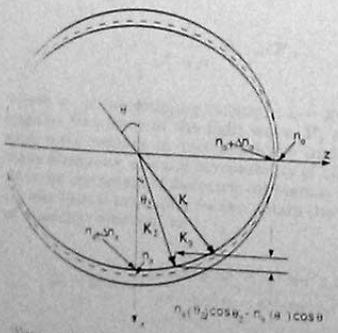

Fig. 4. Wave vectors and modulation scheme of an x-cut $LiNbO_3$ grating.

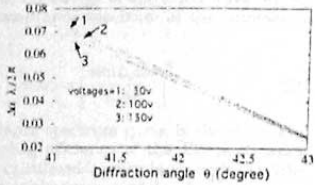

Fig. 6. Relationship between $\Delta\alpha\lambda/2\pi$ and diffraction angle.

the diffraction efficiency of 100% can be realized theoretically. Then with Eqs. (11a), (11b) and (13), we obtain the distribution curves of $\Delta\alpha\lambda/2\pi = [n_e(\theta_2)\cos\theta_2 - n_e(\theta_2)\cos\theta_1]$ as a function of the diffraction angle θ_2, as shown in Fig. 6. Note that $\Delta\alpha\lambda/2\pi = [n_e(\theta_2)\cos\theta_2 - n_e(\theta_2)\cos\theta_1]$ is always larger than 0, which means that the momentum matching condition defined by Eqs. (12) and (13) among the three vectors $\mathbf{K}_1$, $\mathbf{K}_2$, and $\mathbf{K}_g$ does not exist at all. However, $\Delta\alpha$ is an important factor in influencing the coupling efficiency in accordance with the Bragg diffraction theory. A bigger $\Delta\alpha$ can induce the multimode coupling, so we have to study the multimode extension of grating coupling from the compensation for the momentum mismatch $\Delta\alpha$.

5. Compensation for Momentum Mismatch and Optimization of Coupling Efficiency

Assuming $A_1(x)$ and $A_2(x)$ are the components of the complex amplitudes of the normalized modes of incident light wave and diffracted light wave in x direction, we have[12]

$$\frac{dA_1(x)}{dx} = -ik_{12}A_2(x)\exp(i\Delta\alpha x), \tag{15a}$$

$$\frac{dA_2(x)}{dx} = -ik_{12}^{*}A_1(x)\exp(-i\Delta\alpha x), \tag{15b}$$

$$k_{12} = \frac{\omega^2\mu}{2\sqrt{\alpha_1\alpha_2}}\mathbf{P}_1\cdot\Delta\varepsilon\mathbf{P}_2, \tag{15c}$$

where k_{12} is the coupling constant, $\omega = 2\pi c/\lambda$ is the angular frequency of the light wave, $\mathbf{P}_1$ and $\mathbf{P}_2$ are unit wave vectors in incident wave and diffracted wave directions, μ is the permeability of $LiNbO_3$, and $\Delta\varepsilon$ is the increment of dielectric constant ε. With Eq. (1) and optical principle, we can obtain the increment of dielectric constant as

$$\Delta\varepsilon = 2\varepsilon_1\varepsilon_2\frac{n_e^2\cos^2\theta_1\Delta n_o - n_o^2\sin^2\theta_1\Delta n_e}{(n_e^2\sin^2\theta_1 - n_o^2\cos^2\theta_1)^2}. \tag{16}$$

Note that here we are discussing the codirectional coupling. The coupled-mode Eqs. (3a) and (3b) are consistent with the energy conservation in x direction, i.e.,

$$\frac{d}{dx}(|A_1|^2 + |A_2|^2) = 0. \tag{17}$$

When $\Delta\alpha$ is large, Eq. (17) cannot be satisfied, and the set of coupling Eqs. (15a), (15b), and (15c) is no longer valid, and the mode extension has to be used to analyze the coupling procedure of grating. In terms of the mode expansion principle, the TE modes of the diffracted optical waves in the region $x \geq 0$ is represented by the sum of the normal modes as[14,15]

$$A_2(x) = \sum_{m=-\infty}^{\infty}\exp(-i\Delta\alpha x)f_{m2}(z), \tag{18}$$

where

$$f_{m2}(z) = h_{m2}(z)/\sqrt{D_{m2}}, \tag{19a}$$

$$D_{m2} = \int_0^{L_e}|h_{m2}(z)|^2dz, \tag{19b}$$

$$h_{m2}(z) = \Delta n_e(\theta_1, x)\exp(-i\beta_{2z}z). \tag{19c}$$

As shown in Fig. 7(a), the diffracted wave represented by Eq. (18) produces an interaction with grating in the region of interaction depth from $-L_e$ to 0. The interaction depth has its inherent spatial frequency spectrum that covers all the diffraction modes and functions as a phase compensation region before the diffracted wave forms all the possible modes. As a phase compensation, this frequency spectrum can be calculated by

$$A_2(\Delta r) = \int_{-L_e/2}^{L_e/2}f_{m2}(z)\exp(-i\Delta r x)dx, \tag{20}$$

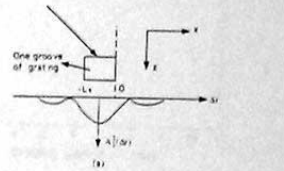

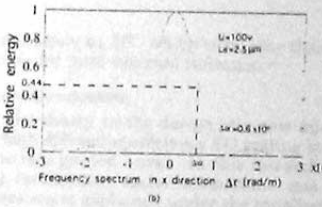

Fig. 7. Frequency spectrum of interaction depth of grating: (a) diffraction theorem; (b) spatial frequency spectrum.

where Δr is the spatial angular frequency in x direction. Then for the energy of diffracted wave, we obtain the transmittance spectrum of the interaction depth as

$$\tau(\Delta r) = \left[\frac{\sin(L_e \Delta r)}{L_e \Delta r}\right]^2. \tag{21}$$

The transmittance spectrum curve is shown in Fig. 7(b). The coupling efficiency of the EO modulation grating can be calculated in accordance with Fig. 7(b), which depends on the compensation of Δr to the mismatch $\Delta\alpha$. For example, when the grating period $\Lambda = 8$ μm, we obtain $\Delta\alpha \approx 0.6 \times 10^6$ from Eq. (13). Then from Fig. 7(b) this corresponds to a transmittance value of approximately 44%. By considering the phase compensation for the mismatch $\Delta\alpha$, one can change the set of coupling Eqs. (15a) and (15b) to

$$\frac{dA_1(x)}{dx} = -ik_{12}A_2(x), \tag{22a}$$

$$\frac{dA_2(x)}{dx} = -ik_{12}^* A_1(x). \tag{22b}$$

Finally we obtain the coupling efficiency of grating as

$$\eta = \left[\frac{\sin(L_e \Delta\alpha)}{L_e \Delta\alpha}\right]^2 \sin^2(k_{12} L_e). \tag{23}$$

As we know, L_e depends on the applied voltage and index modulation $\Delta n_o(\theta_1)$, which again is induced by the applied voltage. Because both the interaction length L_e and the index modulation $\Delta n_o(\theta_1)$ depend on the applied voltage and k_{12} functions as both the index modulation $\Delta n_o(\theta_1)$ and the diffraction angle θ_2, we must optimize the coupling efficiency by taking into account the total contribution from all the important parameters as follows:

$$k_{12} = \frac{4\pi^2 n_o n_e n_o^3 \cos^2\theta_1 \Delta n_e + n_e^3 \sin^2\theta_1 \Delta n_o}{\lambda^2 \sqrt{\alpha_1 \alpha_2}\,(n_e^2 \sin^2\theta_1 + n_o^2 \cos^2\theta_1)^2} \times \cos(\theta_1 - \theta_2), \tag{24}$$

$$L_e = \int_{-L_e}^{0} k_{12}\,dx, \tag{25}$$

$$k_{12}\,dx = \frac{4\pi^2 n_o^4 n_e^4 \cos(\theta_1 - \theta_2)}{\lambda^2 (n_e^2 \sin^2\theta_1 + n_o^2 \cos^2\theta_1)^2 \sqrt{\alpha_1 \alpha_2}} \times (r_{33}\cos^2\theta_1 + r_{13}\sin^2\theta_1) \int_{-L_e}^{0} E_z\,dx. \tag{26}$$

With Eqs. (23)–(26) we obtain the coupling efficiency curve as shown in Fig. 8. We can find from this figure that, when Λ equals approximately 8 μm (as we selected in our project), the coupling efficiency η is approximately 20%. In this simulation, we use the applied voltage of 100 V. According to Fig. 4, the diffraction angle corresponding to the period value of

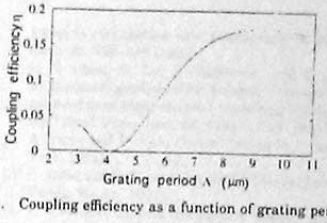

Fig. 8. Coupling efficiency as a function of grating period.

8 μm is approximately 41.35°, which is smaller than the critical angle for total internal reflection.

6. Summary and Conclusions

We report on the theory in the design of a new microstructural high diffraction efficiency EO grating by the use of substrate guided wave. In this research, the operating mechanism under momentum mismatch of the system is explained under the coupling theory, and the coupling efficiency is calculated in the modified formula. In addition, the relation of the periodicity and the diffraction angle is delineated, and the relationship of the grating period of the EO grating and momentum mismatch in the vertical direction $\Delta\alpha$ is discussed. The most important aspect in this research is a new conclusion that a grating coupler requires only the momentum match in the direction of the grating vector, i.e., $\Delta\beta = 0$, whereas in the perpendicular direction of the grating vector, the mismatch $\Delta\alpha$ can be compensated by the mode expansion and Fourier transform of the diffracted wave for the effective interaction depth. With the method in which the interaction depth can be controlled, this research numerically optimizes the coupling efficiency of the EO grating and the expected results are obtained.

The authors thank T. C. Lee and his fellows for their helpful discussions on this research. We also thank Maggie Li and Huajun Tang for their help with this research. This research is currently sponsored by the Office of Naval Research, the Defense Advanced Research Projects Agency, and the advanced technology program of the State of Texas.

References

1. E. G. Paek, P. F. Liao, and H. Gharavi, "Derivation of neural network models and their computational circuits for associative memory," Opt. Eng. **31**, 986–994 (1992).
2. D. G. Sun, L. M. He, N. X. Wang, and Z. H. Weng, "Optoelectronic butterfly interconnection architecture of modified signed-digit arithmetic systems: fully parallel adder and subtracter," Appl. Opt. **33**, 6755–6761 (1994).
3. D. G. Sun, N. X. Wang, L. M. He, Z. W. Lu, and Z. H. Weng, "Butterfly interconnection networks and their applications in digital computing and information processing: applications in FFT-based optical processing," Appl. Opt. **32**, 7184–7193 (1993).
4. A. Neyer, "Electro-optic X-switch using single mode Titanium Lithium Niobate channel waveguides," Electron. Lett. **19**, 553–554 (1993).

5. C. S. Tsai, S. Kim, and F. R. El-Akkari, "Optical channel waveguide switch and coupler using total internal reflection," IEEE J. Quantum Electron. **QE-14**, 513–517 (1978).
6. R. V. Schmidt and P. S. Cross, "Efficient optical waveguide switch amplitude/modulator," Opt. Lett. **2**(2), 45–47 (1978).
7. O. H. Kitani, S. Namba, and M. Kawabe, "Electro-optic Bragg deflection modulators in corrugated waveguides," IEEE J. Quantum Electron. **QE-15**(5), 270–272 (1979).
8. R. T. Chen, M. R. Wang, G. J. Sonek, and T. Jannson, "Optical interconnection using polymer microstructure waveguides," Opt. Eng. **30**, 622–628 (1990).
9. R. T. Chen, M. R. Wang, and T. Jannson, "Intraplane guided wave massive fanout optical interconnections," Appl. Phys. Lett. **57**, 2071–2073 (1990).
10. R. T. Chen, H. Lu, D. Robinson, Z. Sun, and J. Jannson, "60 GHz board-to-board interconnection using polymer optical buses in conjunction with microprizm couplers," Appl. Phys. Lett. **60**, 536–538 (1992).
11. R. T. Chen, H. Lu, D. Robinson, and T. Jannson, "Highly multiplexed graded-index polymer waveguide hologram for near-infrared eight-channel wavelength division demultiplexing," Appl. Phys. Lett. **59**, 1144–1146 (1991).
12. A. Yariv and P. Yeh, *Optical Waves in Crystals* (Wiley, New York, 1984).
13. P. Moon and D. E. Spencer, *Field Theory Handbook* (Springer-Verlag, Berlin, 1971).
14. K. Koshiba, *Optical Waveguide Theory by the Finite Element Method* (KTK Science Publishers, Tokyo, 1992), pp. 162–166.
15. M. Li and S. J. Sheard, "Waveguide couplers using parallelogramic-shaped blazed gratings," Opt. Commun. **109**, 239–245 (1994).